Journal of Hazardous Materials 431 (2022) 128534

Contents lists available at ScienceDirect

Journal of Hazardous Materials

journal homepage: www.elsevier.com/locate/jhazmat

Research Paper

Sulfidation extent of nanoscale zerovalent iron controls selectivity and reactivity with mixed chlorinated hydrocarbons in natural groundwater

Marco C. Mangayayam [a], Jeffrey Paulo H. Perez [b,c], Virginia Alonso-de-Linaje [d,e], Knud Dideriksen [f], Liane G. Benning [b,c], Dominique J. Tobler [a,g,*]

[a] Nano-Science Center, Department of Chemistry, University of Copenhagen, Universitetsparken 5, 2100 Copenhagen, Denmark
[b] GFZ German Research Centre for Geosciences, Telegrafenberg, 14473 Potsdam, Germany
[c] Department of Earth Sciences, Freie Universität Berlin, 12249 Berlin, Germany
[d] AECOM Environment Madrid, Spain
[e] GIR-QUESCAT, Departamento de Quimica Inorgánica, Universidad de Salamanca, Salamanca, Spain
[f] Geological Survey of Denmark & Greenland (GEUS), Øster Voldgade 10, 1350 Copenhagen, Denmark
[g] Department of Plant and Environmental Sciences, University of Copenhagen, 1871 Frederiksberg C, Denmark

HIGHLIGHTS

- Effect of sulfidation on reactivity of nZVI with a complex mixture of chlorinated hydrocarbons (CHCs) in groundwater.
- Sulfidation time increases thickness of the mackinawite-rich S-nZVI shell, affecting the degradation of CHCs.
- TCE, PCE, trans-DCE and 1,1-DCE were reduced fastest when FeS sites were most abundant.
- cis-DCE, 1,1,2-TCA and TCM were reduced fastest when Fe^0/FeOx sites became accessible upon aging.

GRAPHICAL ABSTRACT

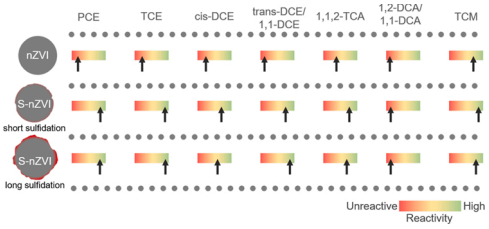

ARTICLE INFO

Editor: Yang Deng

Keywords:
Corrosion
Metallic iron
Remediation
Iron sulfide
Chlorinated ethenes, ethanes and methanes

ABSTRACT

Sulfidated nanoscale zerovalent iron (S-nZVI) exhibits low anoxic oxidation and high reactivity towards many chlorinated hydrocarbons (CHCs). However, nothing is known about S-nZVI reactivity once exposed to complex CHC mixtures, a common feature of CHC plumes in the environment. Here, three S-nZVI materials with varying iron sulfide (mackinawite, FeS_m) shell thickness and crystallinity were exposed to groundwater containing a complex mixture of chlorinated ethenes, ethanes, and methanes. CHC removal trends yielded pseudo-first order rate constants (k_{obs}) that decreased in the order: trichloroethene > trans-dicloroethene > 1,1-dichlorethene > trichloromethane > tetrachloroethene > cis-dichloroethene > 1,1,2-trichloroethane, for all S-nZVI materials. These k_{obs} trends showed no correlation with CHC reduction potentials based on their lowest unoccupied molecular orbital energies (E_{LUMO}) but absolute values were affected by the FeS_m shell thickness and crystallinity. In comparison, nZVI reacted with the same CHCs groundwater, yielded k_{obs} that linearly correlated with CHC E_{LUMO} values ($R^2 = 0.94$) and that were lower than S-nZVI k_{obs}. The CHC selectivity induced by sulfidation treatment is explained by FeS_m surface sites having specific binding affinities towards some CHCs, while others require access to the metallic iron core. These new insights help advance S-nZVI synthesis strategies to fit specific CHC treatment scenarios.

* Corresponding author at: Department of Plant and Environmental Sciences, University of Copenhagen, 1871 Frederiksberg C, Denmark.
E-mail address: dominique.tobler@plen.ku.dk (D.J. Tobler).

https://doi.org/10.1016/j.jhazmat.2022.128534
Received 24 August 2021; Received in revised form 25 January 2022; Accepted 19 February 2022
Available online 22 February 2022

1. Introduction

Chlorinated hydrocarbons (CHCs) have been intensively used as industrial solvents (Lawrence, 2006), and their improper disposal has resulted in CHC contaminated soils and groundwater (Moran et al., 2007). In anaerobic subsurface environments, CHCs often undergo sequential degradation by dehalogenating microbial consortia and Fe (II)-bearing soil minerals, which often leads to partially dehalogenated compounds (e.g., dichloroethene, vinyl chloride) that degrade much slower (Middeldorp et al., 1999). As a result, CHC contaminant plumes are often characterized by a complex mixture of variably degraded CHCs that will persist and continuously dissolve into the groundwater (Barrio-Lage et al., 1986). Over the past three decades, zerovalent iron (ZVI) has been regarded as the state-of-the-art reactant for in situ groundwater remediation of CHCs (Phenrat et al., 2019; Stefaniuk et al., 2016; Vogan et al., 1999; Mueller et al., 2012). However, ZVI is non-selective and reacts with many non-target compounds including water, traces of dissolved oxygen and common groundwater solutes (e.g., nitrate), which consumes electrons of the metallic iron, Fe^0 (i.e., reduces its electron efficiency), and quickly leads to the formation of a passivating iron (oxyhydr)oxide (FeOx) shell (Bae et al., 2018; Reardon 2005). This is particularly true for nanoscale ZVI (nZVI), which due to its small size (generally $>$ 100 nm) have much enhanced surface area.

Several surface modifications of nZVI have been proposed to augment fast anoxic oxidation by water and non-target solutes in order to enhance selectivity towards the target contaminants. Sulfidation of nZVI (S-nZVI), wherein a sulfur reagent is added during or after nZVI synthesis (i.e., one-step or two-step synthesis), has emerged as a promising approach (Kim et al., 2011; Rajajayavel and Ghoshal 2015). Coating nZVI with an iron sulfide (FeS_x) rich shell selectively facilitates the electron transfer from the Fe^0 core to the target contaminants (e.g., CHCs) while protecting the core from fast anoxic oxidation (Fan et al., 2016; Nunez Garcia et al., 2021; He et al., 2018; Mangayayam et al., 2019a; Xu et al., 2019). In addition, a number of studies show that S-nZVI has similar or multi-fold higher rates of CHC degradation relative to nZVI (Kim et al., 2011; Rajajayavel and Ghoshal 2015; Fan et al., 2016; Zhang et al., 2021). This sulfidation induced enhancement in nZVI reactivity with CHC is argued to result from the increased electrical conductivity and increased hydrophobicity induced by the FeS_x rich shell (Kim et al., 2011; Mangayayam et al., 2019a; Xu et al., 2019; Xu et al., 2020; Gu et al., 2017). In addition, the FeS_x shell not only forms a physical barrier between water and the Fe^0 core, but sulfur itself is also argued to block H adsorption and H_2 dissociation (Xu et al., 2019; Burke and Madix 1990; Bartholomew et al., 1982). Thus, sulfidation drastically limits anoxic oxidation, which in turn increases electron efficiency towards CHCs.

So far, the majority of S-nZVI studies have used trichloroethylene (TCE) as model CHC compound to assess how S-nZVI reactivity is controlled by the various sulfidation treatment and to identify the bulk and surface S-nZVI properties that lead to highest dechlorination rates. A recent review by Nunez Garcia et al., (2021) presented an overview of 108 peer-reviewed studies of S-nZVI and S-mZVI (microscale ZVI) reactivity with various contaminants, where 37 studies assessed rates of TCE reduction. However, as mentioned earlier, contaminant plumes often contain multiple CHCs, but only a few studies have analysed how sulfidation treatment affects the degradation of CHC other than TCE (Nunez Garcia et al., 2021). Moreover, so far, S-nZVI reactivity with CHC has only been studied in single CHC systems (Rajajayavel and Ghoshal, 2015; Fan et al., 2016; Nunez Garcia et al., 2021; Zhang et al., 2021), and there is only one field study that investigated the reactivity of S-nZVI at a contaminated site where multiple CHCs were present (Nunez Garcia et al., 2020). While this field study successfully demonstrated the reduction of PCE, TCE, cis-DCE by S-nZVI in the subsurface, the data gives little insight into how sulfidation treatment affects nZVI reactivity in contact with mixed CHCs. Thus, it is unknown to what extent CHCs compete with each other for reactive sites on the FeS_x rich surface of S-nZVI materials, and how this affects individual dechlorination rates and extent. Identifying the degree of co-contaminant competition is key in the further optimisation of S-nZVI materials and ultimately for the design of S-nZVI treatment strategies for the clean up of complex CHC plumes.

To investigate CHC competitive effects, a groundwater contaminated with chlorinated ethenes, ethanes, and methanes was collected from a Spanish industrial site and exposed to S-nZVI and nZVI to determine dechlorination rates and extents for the individual CHC compounds. In addition, three different S-nZVI materials were tested differing in sulfidation treatment (i.e., varied nZVI exposure to Na_2S reagent: 0.25, 2.5 and 25 h). Prior exposure, nZVI and S-nZVI materials were characterised with high energy X-ray diffraction (HEXRD), (scanning) transmission electron microscopy (S/TEM), and X-ray photoelectron spectroscopy (XPS) to assess differences in shell architecture to help interpret results from CHC competition studies. For the first time, we give insights into how sulfidation affects competition between CHCs for reduction by nZVI, which in turn allows us to start thinking of tailored S-nZVI synthesis protocols towards specific in-situ CHC treatment scenarios.

2. Materials and methods

Unless specified, material synthesis and preparation for characterization and reactivity experiments were done in a Coy anoxic glovebox (95% N_2/ 5% H_2) using following chemicals: $FeCl_2{\cdot}4\ H_2O$ (99+%, Acros Organics), $NaBH_4$ (98%, Sigma Aldrich), sodium acetate (Reagent grade, Sigma Aldrich), acetic acid (99%, Reagent plus), HCl (37%, Sigma Aldrich), and $Na_2S{\cdot}9\ H_2O$ (98+%, Sigma Aldrich).

2.1. Material Synthesis and Characterization

Nanoscale ZVI (nZVI) was synthesized using the borohydride method as described in our previous study (SI, Text S1) (Mangayayam et al., 2019a). Three different S-nZVI materials were prepared by exposing freshly synthesized nZVI to a Na_2S solution (S/Fe_{dosed}: 0.23) for different time lengths (i.e., 0.25, 2.5 and 25 h). After synthesis, the solids were collected using a strong magnet, washed with O_2-free ethanol thrice, and vacuum filtered. The resulting solids were immediately used for reactivity experiments in the groundwater (Section 2.2) or prepared for material characterization by HEXRD, XPS and TEM (detailed information can be found in SI, Text S2). In brief, HEXRD patterns of dried, anoxic materials were obtained at beamline 11-ID-B at Advanced Photon Source (USA) using a 40 $\times$ 40 amorphous Si detector placed 1000 mm away from the sample. Data correction, normalisation and transformation to 1-D diffraction pattern were done following previously reported procedures (Mangayayam et al., 2019b). S/TEM images and EDX maps were collected using an FEI Tecnai G2 F20 X-Twin S/TEM equipped with a Gatan imaging filter (GIF) Tridiem™, a Fischione high angle annular dark field (HAADF) detector and an EDAX X-ray analyzer. XPS analyses were performed using a Kratos Axis Ultra XPS under ultrahigh vacuum (10^{-9} Pa). Spectral analyses were done in the CasaXPS software.

2.2. S-nZVI and nZVI reactivity with groundwater

The CHC contaminated groundwater was collected from a monitoring well at a Spanish industrial site and characterized as done in our previous work (Alonso-de-Linaje et al., 2019). It contained perchloroethene (PCE), trichloroethene (TCE), trans-dicloroethene (trans-DCE), cis-dichloroethene (cis-DCE), 1,1-dichlorethane (1,1-DCA), 1,2-dichlorethane (1,2-DCA), 1,1,2-trichloroethane (1,1,2-TCA), tetrachloromethane (CT) trichloromethane (TCM), and vinyl chloride (VC). The geochemical composition including the various CHC concentrations are given in Table 1. Until use, the collected groundwater was stored at 4 °C, inside fully filled 1-liter glass bottles (i.e., no headspace). Duplicate reactivity experiments with the CHC contaminated

groundwater were set up for each S-nZVI material (2 x 3 = 6 reactors) and for nZVI (2 reactors) and duplicate control experiments with groundwater only were set-up in parallel. For this, the synthesised material was resuspended in 150 mL groundwater inside 160 mL serum bottle and then capped with Viton™ rubber stoppers to give a final mass loading of 1 g L^{-1}. The bottles were mixed on an orbital shaker at 150 rpm for 45 days. Additional reactors containing S-nZVI and only one or two CHC compounds (i.e., cis-DCE, TCE and 1,1,2-TCA) were set-up to test CHC competitive reactions, specific site reaction, and daughter product formation (specifics given in SI, Text S3). For these single/dual CHC-containing experiments, the groundwater was first sparged with N_2 overnight to remove all the initial CHC contents while keeping all non-volatile groundwater solutes. The sparged groundwater was then amended with one or two CHCs to match their concentration in the groundwater (further details given in SI, Text S3).

Suspension samples (1 mL) were regularly removed from all experimental and control reactors for headspace gas chromatography mass spectrometry (GC-MS) analysis. For this, collected samples were mixed with 9 mL of degassed MilliQ water inside a sealed 20 mL GC glass vial and then analyzed using an Agilent 6890 with a Gerstel 1888 Autosampler. Prior to headspace extraction, the vials were equilibrated for 15 min at 50 °C. One µL of headspace was injected onto a DB-624MS (Agilent) column, set at 35 °C and then heated to 115 °C at a rate of 10 °C min^{-1} (Mangayayam et al., 2019b). Normalized concentrations (C/C_o) were calculated by dividing concentrations in the experimental reactor with concentrations in the control reactor (without reactant materials) and the data fit using pseudo first-order kinetics (Mangayayam et al., 2019b):

$$ln\left(\frac{C}{C_o}\right) = -kt$$

The analytical error was determined by multiplying the individual measurement with the % uncertainty (as determined from the corresponding duplicate measurement), and this was always < 5% relative.

Table 1
Geochemistry and physicochemical parameters of the groundwater collected at a Spanish industrial site. Uncertainties refer to instrumental errors.

Inorganic solutes	Symbol	(mg L^{-1})
Calcium	Ca^{+}	120
Potassium	K^{+}	2.6
Sodium	Na^{+}	220
Chlorine	Cl^{-}	280
Carbonate	CO_3^{2-}	< 5.0
Bicarbonate	HCO_3^{-}	300
Sulphate	SO_4^{2-}	130
Nitrate	NO_3^{-}	6.5
Organic solutes	**Abbrev.**	**(µg L^{-1})**
Tetrachloroethylene	PCE	330 ± 30
Trichloroethylene	TCE	1500 ± 165
1,1-dichloroethylene	1,1-DCE	180 ± 30
Cis-dichloroethylene	cis-DCE	380 ± 40
Trans-dichloroethylene	trans-DCE	440 ± 90
Vinyl chloride	VC	51 ± 10
1,1,2-trichloroethane	1,1,2-TCA	7800 ± 860
1,1-dichloroethane	1,1-DCA	600 ± 90
1,2-dichloroethane	1,2-DCA	1500 ± 225
Tetrachloromethane	CT	31 ± 3
Trichloromethane	TCM	3200 ± 380
Other parameters		
pH		7.02
Conductivity (µm/cm)		1949
E_h (mV)[a]		156
Total organic carbon (mg L^{-1})		8.2

[a] referenced to standard hydrogen electrode (mV)

3. Results and discussion

3.1. Initial nZVI and S-nZVI characterization

The HEXRD patterns of the S-nZVI materials sulfidated for 0.25, 2.5 and 25 h (hereafter referred to as S-$nZVI_{0.25\,h}$, S-$nZVI_{2.5\,h}$, and S-$nZVI_{25\,h}$) were comparable to non-sulfidated nanoscale ZVI (nZVI) except for an additional peak at Q = 1.19 $Å^{-1}$ (*d*-spacing = 3.27 Å, Fig. S1), which corresponds to an expanded basal spacing of the nanocrystalline mackinawite shell, FeS_m (001) (Mangayayam et al., 2019a). No other FeS_x phases or FeOx phases were detected in the patterns. The full-width at half maximum (FWHM) of the FeS_m (001) peak decreased with increasing sulfidation time (Fig. S1), suggesting an increased FeS_m shell crystallinity along the [001] direction with increased exposure to the sulfide solution. This increased structural ordering with sulfidation time was also apparent in HRTEM images that showed S-$nZVI_{25\,h}$ shells with lattice fringes with interlayer distance of about 5 Å (Fig. 1), corresponding to the interlayer basal spacing of FeS_m sheets (Mangayayam et al., 2019a). In comparison, S-$nZVI_{0.25\,h}$ exhibited similar but fewer and less well-developed lattice fringes (Fig. 1). Notably, S-$nZVI_{0.25\,h}$ had a significantly thinner effective shell layer (4.3 ± 0.8 nm) compared to S-$nZVI_{25\,h}$ (9.2 ± 3.5 nm), as indicated by the particle analysis of the TEM images (Fig. S2; *p*-value < 0.00001, Tukey's HSD). Moreover, EDX maps and line intensity profiles also showed that S-$nZVI_{0.25\,h}$ exhibited a lower sulfur intensity at the interface compared to S-$nZVI_{25\,h}$ (Fig. 1). In agreement with HRTEM images and EDX maps, XPS measurements revealed direct proportionality between the surface S/Fe atomic ratios and sulfidation time, suggesting increasing FeS_m shell thickness with increasing sulfidation time (Table S1). The XPS data also showed that the dominant sulfur specie in all S-nZVI materials was sulfide, S^{2-} (~77–81% of detected sulfur), while disulphide, S_2^{2-}, and polysulfide species, S_n^{2-}, were minor phases (< 20%, Table S2). Noteworthy that XPS wide scans of S-nZVI materials showed an increase in oxygen content with an increase in sulfidation time (Table S1). However, this should not be mistaken for an increase in oxidised Fe and S species, as we saw no clear indication for this in the high resolution XPS scans for S 2p and Fe 2p (Fig. S3), and HEXRD also showed no peaks for any FeO_x phases (Fig. S1). Also note that the amount of Fe decreased with increasing sulfidation (Table S1), suggesting that the amount of Fe^0 was lower in the surface region of the more sulfidated S-nZVI, $SnZVI_{25\,h}$. Our complementary results from HEXRD, S/TEM, and XPS analyses confirmed that all three S-nZVI types exhibited a FeS_m shell, but the shell thickness and crystallinity along the {001} direction substantially increased with sulfidation time (i.e., the FeS_m density per unit area increases). Note that although mean particle diameters of the three S-nZVI materials increased slightly from 87.4 ± 21.4 nm (S-$nZVI_{0.25\,h}$) to 92.8 ± 24.6 (S-$nZVI_{25\,h}$), as shown by particle analysis in TEM images (Fig. S4), these values are not significantly different ($p = 0.25$, One-way ANOVA). Given that particle morphologies between these S-nZVI materials were almost identical and no secondary material was observed (Fig. S5), the particle surface area will not have varied significantly, as shown by the estimated geometric surface areas (between 13.5 and 14.3 $m^2\ g^{-1}$).

Previous studies that investigated the shell composition and structure of two-step synthesised S-nZVI also highlighted that a poorly crystalline FeS phase forms around the nZVI core and that its thickness increases with increasing S/Fe_{dosed} (Brumovský et al., 2020). However, in recent studies that investigated the effect of sulfidation time on S-nZVI shell properties, they often observed the secondary precipitation of flake-like FeS with increasing sulfidation (Fan et al., 2016; Xu et al., 2019), which is absent here (Fig. S5). This may be due to differences in applied S/Fe_{dosed} and sulfidation approach, which is also supported by the fact that they generally observed equal or an even higher abundance of disulfide species compared to sulfide species (Xu et al., 2019), while for S-nZVI materials in this study, the amount of disulfide species in the shell was small (Table S2). The mean particle diameter and surface area

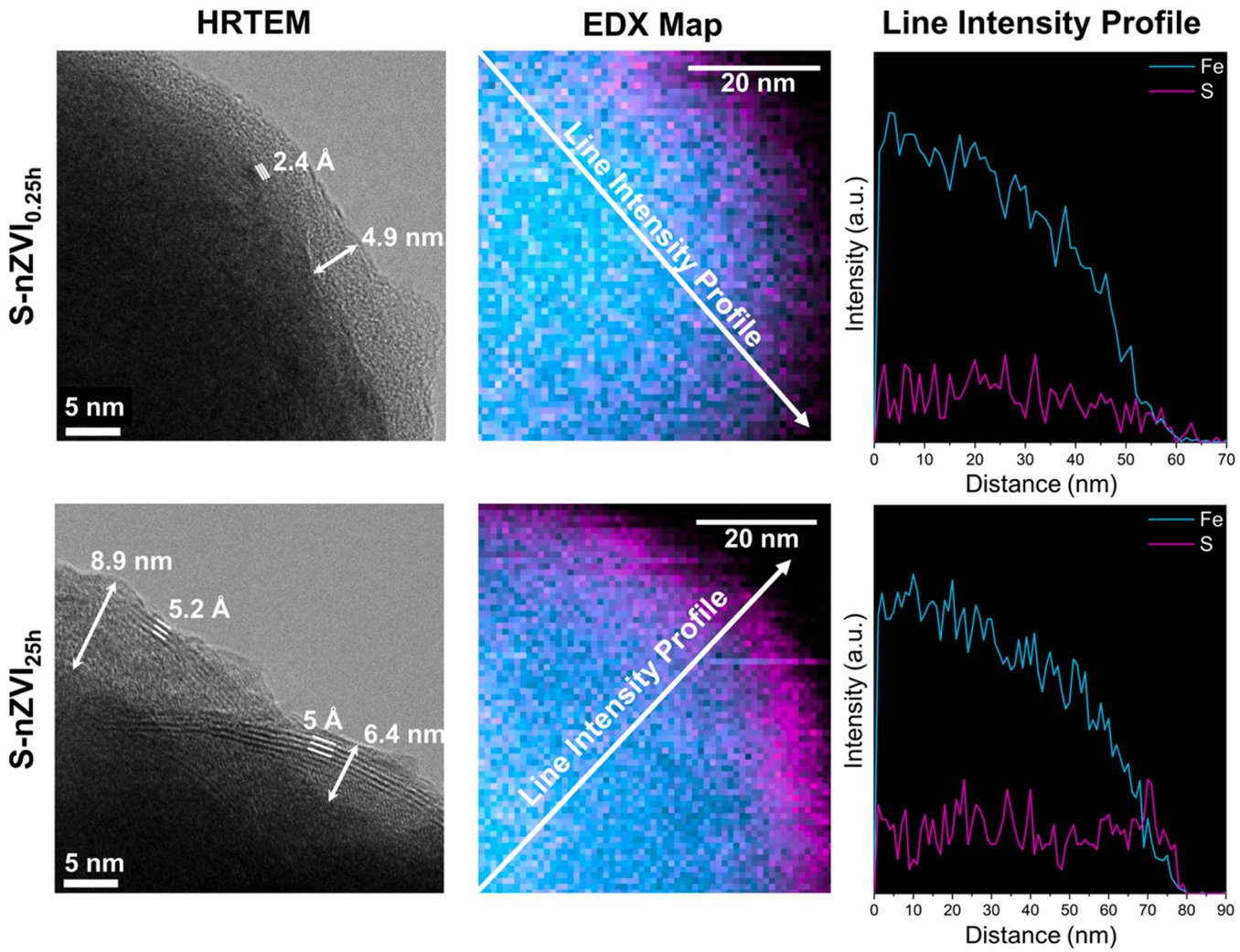

Fig. 1. HRTEM and EDX map with line intensity profile (white arrow in EDX map) showing the variability in FeS_m shell thickness for the two S-nZVI materials, S-$nZVI_{0.25\ h}$ (short sulfidation) and S-$nZVI_{25\ h}$ (long sulfidation). The arrows in HRTEM images show the effective thickness of the shell layer (i.e., low contrast features of the particle interface). Lattice fringes with interlayer spacing of 2 Å observed in S-$nZVI_{0.25\ h}$ indicate {110} of Fe^0, while the lattice fringes with interlayer spacing of 5 Å observed in S-$nZVI_{25\ h}$ correspond to {001} of FeS_m.

of S-nZVI materials in this study are in line with previous S-nZVI studies that applied a similar sulfidation technique (Nunez Garcia et al., 2021).

Based on recent S-nZVI surface and bulk characterisation studies (Nunez Garcia et al., 2021; Xu et al., 2019, 2020; Cao et al., 2021), the observed increase in the thickness and crystallinity of the FeS_m shell with increasing sulfidation time, will likely impact positively on S-nZVI electrical conductivity and surface hydrophobicity, and also more effectively block the adsorption of H and H_2 dissociation (i.e., inhibit anaerobic oxidation). Overall, we would therefore expect the S-nZVI material with the more crystalline FeS_m shell, S-$nZVI_{25\ h}$, to have a higher electron efficiency for CHC compared to S-$nZVI_{0.25\ h}$. In contrast, S-nZVI materials with a lower FeS_m shell crystallinity and thickness likely exhibit a higher amount of defects and thus a higher variability in surface sites, potentially also give access to Fe^0/FeO_x surface sites, which could promote several reduction pathways (i.e., hydrogenolysis on Fe^0 sites and β elimination on FeS_m sites), thus favouring the degradation of multiple CHCs at once, at the cost of electron loss to anaerobic oxidation.

3.2. Reduction of CHCs by nZVI (reference system)

As a benchmark for S-nZVI reactivity, we investigated the reduction of CHCs by non-sulfidated nZVI in the collected groundwater. The pseudo-first order rate constants, k_{obs} (h^{-1}), derived from fitting the decrease in normalised CHC concentration with time, followed the order: TCM > 1,1,2-TCA > PCE > TCE > trans-DCE > cis-DCE (Fig. 2; Table S3). No reaction was seen with 1,1-DCA and 1,2-DCA. Previous studies also observed little if any 1,2-DCA reduction by nZVI (Song and Carraway, 2005; Nunez Garcia et al., 2016), while for 1,1-DCA, reduction rates were generally very low and it required extended monitoring time to observe 1,1-DCA degradation, which may explain it was not observed here. Also, Velimirovic et al., (2013) showed that not all ZVI materials react with 1,1-DCA, so this reaction is also highly dependent on the properties of the synthesised ZVI material.

3.3. Reduction of CHCs by S-nZVI

3.3.1. Chlorinated ethenes

PCE, TCE, trans-DCE and 1,1-DCE were reduced faster by S-nZVI materials that were sulfidated for longer (Fig. 2a-d), i.e., k_{obs}(S-$nZVI_{25\ h}$) > k_{obs}(S-$nZVI_{2.5\ h}$) > k_{obs}(S-$nZVI_{0.25\ h}$) (Table S3), suggesting that the reduction rates of these compounds increased with increasing FeS_m shell thickness and crystallinity. Note that it is very unlikely that the observed variations in k_{obs} between S-nZVI materials discussed here and below resulted from variations in surface area because we observed almost identical mean particle sizes (Fig. S4) and particle morphologies (Fig. S5) for these three S-nZVI materials. Further note that the k_{obs}

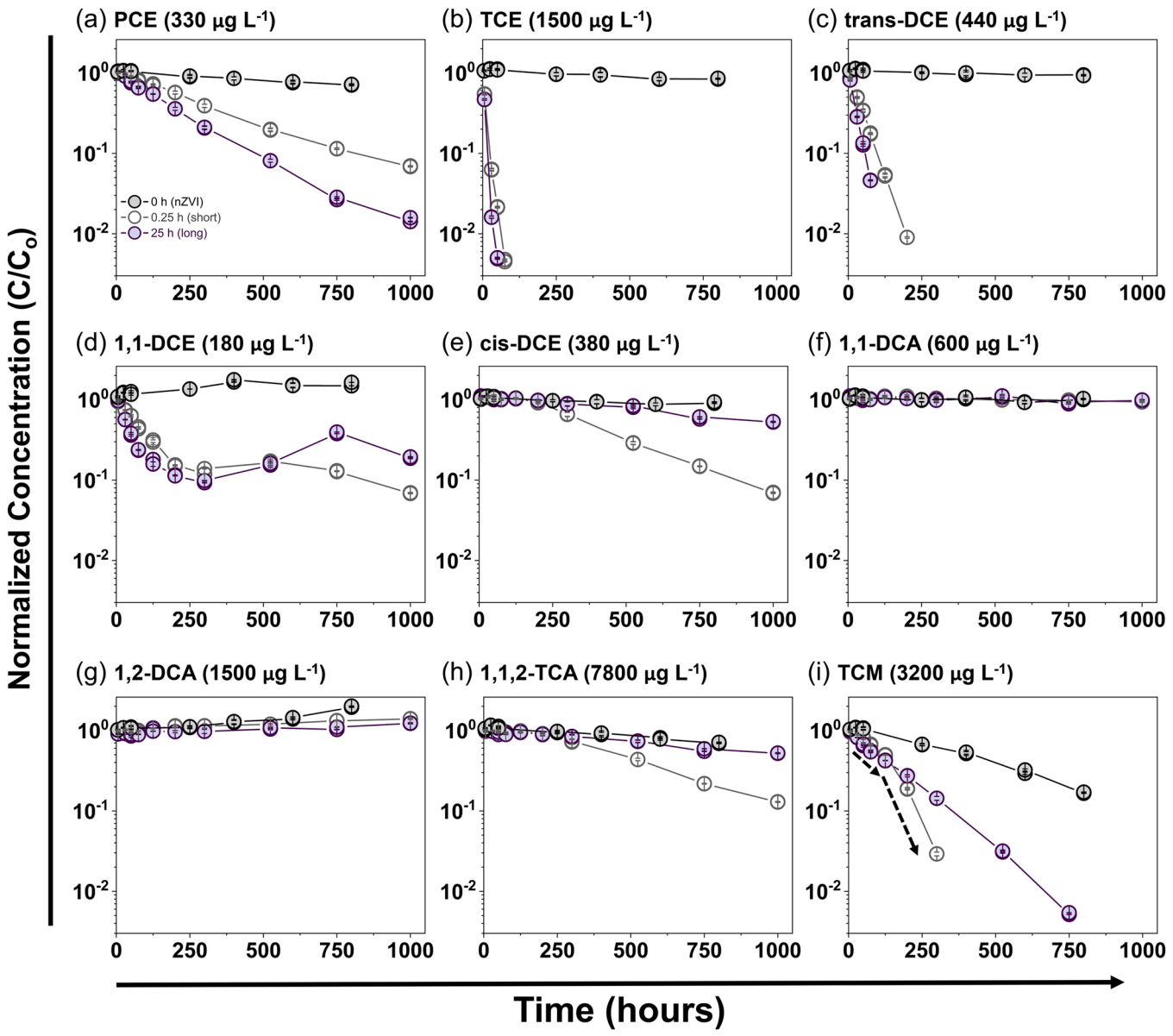

Fig. 2. Time-dependent decrease in normalized CHC concentrations (with C_0 denoting CHC concentrations in control experiments) upon reaction with non-sulfidated nZVI, S-nZVI$_{0.25\ h}$ and S-nZVI$_{25\ h}$ (y-axis in log scale). (a) PCE, (b) TCE, (c) trans-DCE, (d) 1,1-DCE, (e) cis-DCE, (f) 1,1,2-TCA, (g) 1,1-DCA, (h) 1,2-DCA, (i) TCM. For clarity, CHC reduction trends by S-nZVI$_{2.5\ h}$ are shown in the Supplementary information (Fig. S6). No concentration time trends could be determined for carbon tetrachloride (CT) and vinyl chloride (VC) due to their low concentration in the collected groundwater and instrumental limitation (Table 1). Note that each condition was tested in duplicate (i.e., two separate reactors), but the two data points may be hard to see due to log scale and high experimental reproducibility. Error bars represent analytical uncertainties (<5% relative).

values for 1,1-DCE were calculated with data collected between 0 and 200 h (Fig. 2d), because 1,1-DCE concentrations started to increase after 300 h monitoring. This increase indicated that 1,1-DCE formed as a daughter product during the dehalogenation of another CHC compound. Amongst these four chlorinated ethenes, TCE was reduced the fastest, followed by trans-DCE, 1,1-DCE and PCE. In a recent study that monitored PCE, TCE, and trans-DCE degradation rates in single CHC reactions (Zhang et al., 2021), they also observed k_{obs} of the same magnitude as in this study, but rates for trans-DCE were highest, followed by TCE and PCE.

For cis-DCE reduction, k_{obs} values decreased with increasing sulfidation time (i.e., increasing FeS_m shell crystallinity and thickness, Fig. 2e, Table S3). Moreover, significant cis-DCE reduction only occurred after a 100-h incubation period, thus k_{obs} values were calculated with data collected after this lag time. A significant delay (~75 h) in cis-DCE reduction was also observed when only cis-DCE (640 µg L^{-1}) was reacted with S-nZVI$_{0.25\ h}$ (single CHC reaction, Fig. 3), indicating that the lag time was not related to the presence of other CHCs. We demonstrated previously that the FeS_m shell of S-nZVI lowered cis-DCE k_{obs}, because it blocked access to Fe^0/FeOx sites needed for cis-DCE reduction (Mangayayam et al., 2019b). We also showed that it required some aging of S-nZVI in pristine groundwater (i.e., a certain incubation period), for Fe^0/FeOx sites to be exposed at FeS_m shell defects, that operate as locally separated anodic and cathodic sites for the gradual oxidation of the Fe^0 core and the formation of H_2 (Mangayayam et al., 2019a). We therefore argue that S-nZVI$_{0.25\ h}$ has a higher cis-DCE k_{obs} compared to S-nZVI$_{25\ h}$ because of its thinner and less crystalline FeS_m shell. This also means it will be more prone to aging effects, and thus will expose Fe^0/FeOx sites more readily leading to higher rates of cis-DCE reduction.

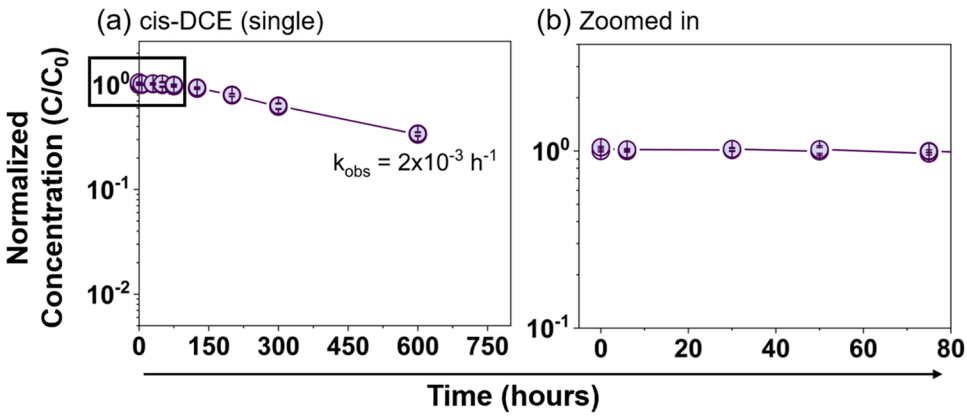

Fig. 3. (a) Time-dependent decrease in normalised cis-DCE concentration (640 μg L^{-1}) in the presence of S-nZVI$_{0.25\ h}$ in single CHC experiment (no other CHC present, but same groundwater matrix) showing little if any reduction during the initial 80 h (framed by rectangular box), which for clarity is zoomed in (b). C_0 denotes the cis-DCE in the control experiment to which no S-nZVI materials were added, and y-axes are shown in log scale. Note that duplicate reactions were performed, but the two data points may be hard to see due to log scale and high experimental reproducibility. Error bars represent analytical uncertainties (<5% relative).

Conversely to this and our previous work (Mangayayam et al., 2019b), a recent study observed favorable effects of sulfidation on cis-DCE degradation rates in single CHC reactions (Zhang et al., 2021), although their k_{obs} was of similar magnitude as the k_{obs} in the S-nZVI$_{0.25\ h}$ reactions here. Likely, their nZVI precursor material was less reactive with cis-DCE compared to the nZVI tested here, while differences in S/Fe$_{dosed}$ ratio and sulfidation treatment and the absence/presence of multiple CHC, likely also contributed to these contrasting observations.

3.3.2. *Chlorinated ethane*

No reduction was observed for 1,1-DCA and 1,2-DCA (Fig. 2f, g), while 1,1,2-TCA reduction was observed following a 200-h incubation period (Fig. 2h), with k_{obs} correlating inversely with sulfidation time, i.e., k_{obs}S-nZVI$_{0.25\ h}$ > k_{obs}S-nZVI$_{2.5\ h}$ > k_{obs}S-nZVI$_{25\ h}$ (Table S3). We performed a separate experiment with S-nZVI$_{25\ h}$ and only 1,1,2-TCA added to identify the cause of the delay. In the absence of other CHCs, we observed instantaneous 1,1,2-TCA reduction with rates higher than the rates measured in the CHCs groundwater (Fig. 4a), suggesting that 1,1,2-TCA can be reduced at the FeS_m sites and that the observed delay in the CHCs groundwater could stem from competition with other CHCs for the same reactive sites. TCE is a likely site competitor because it was reduced the fastest within the first 100 h (Fig. 2b). This was reaffirmed in a separate batch reactor, where S-nZVI$_{25\ h}$ was reacted only with 1,1,2-TCA and TCE (at identical concentrations as in CHCs groundwater), which showed that TCE was reduced instantaneously and at comparable rates (0.10 ± 0.01 h^{-1}) as observed in the CHCs groundwater (0.11 ± 0.01 h^{-1}), while the reduction of 1,1,2-TCA was delayed, with significant reduction only measured after ≥ 100 h (Fig. 4b). Moreover, the delay in 1,1,2-TCA reduction matched the time span required for TCE to be completely removed (i.e., could no longer be detected, Fig. 4b). Thus, if TCE and 1,1,2-TCA co-exist in a contaminated groundwater, TCE will be reduced first by S-nZVI because it is favored over 1,1,2-TCA at the FeS_m sites. It is important to note that 1,1,2-TCA

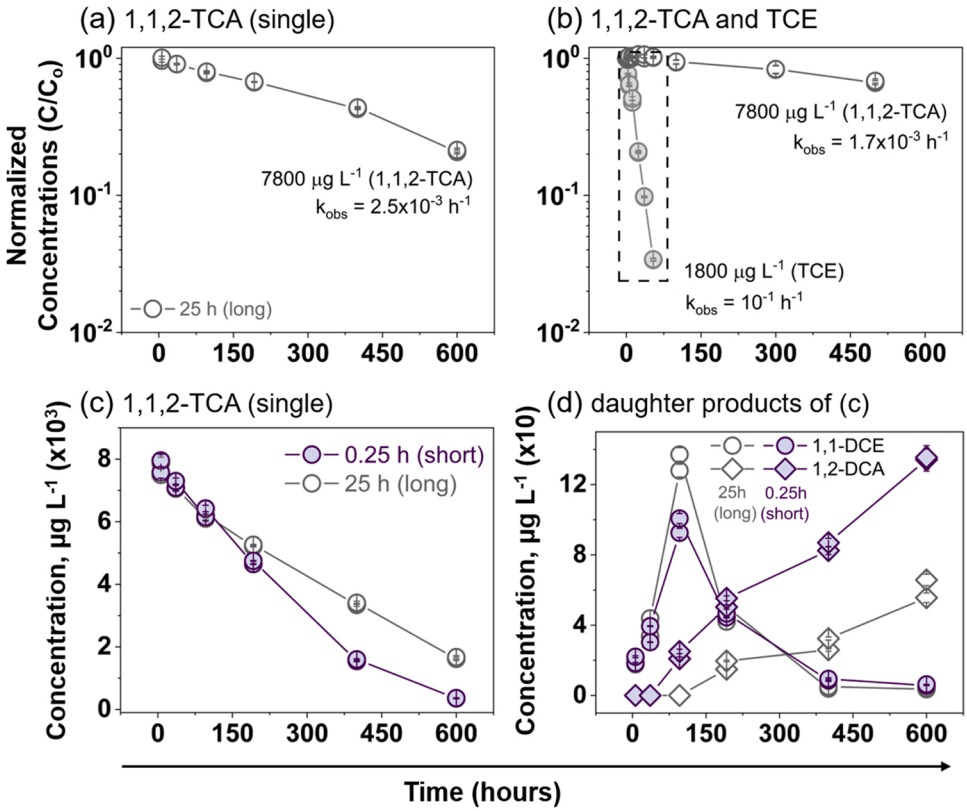

Fig. 4. (a) Single 1,1,2-TCA (7800 μg L^{-1}) and b) dual 1,1,2-TCA (7800 μg L^{-1}) and TCE (1800 μg L^{-1}) reduction experiments in the presence of S-nZVI$_{25\ h}$ with no other added CHCs (C_0 denotes concentration in control experiment; y-axis in log scale). The marked box in (b) highlights the time frame, where TCE was actively reduced, while 1,1,2-TCA reduction seemed negligible. (c) Comparison of 1,1,2-TCA removal trends between S-nZVI$_{25\ h}$ and S-nZVI$_{0.25\ h}$ in single CHC experiments and d) the observed formation of daughter products, 1,2-DCA and 1,1-DCE. Note that each condition was tested in duplicate (i.e., two separate reactors), but the two data points may be hard to see due to log scale and high experimental reproducibility. Error bars represent analytical uncertainties (<5% relative).

likely also competes with other CHCs, particularly trans-DCE, which is also quickly degraded within the first 200 h; an aspect that should be tested in future experiments.

1,1,2-TCA degradation by S-nZVI is suggested to proceed via direct electron transfer to form non-chlorinated hydrocarbons (Zhang et al., 2021). In addition, we also identified the formation of minor amounts of 1,2-DCA and 1,1-DCE (i.e., corresponding to 2–4% of 1,1,2-TCA transformation), which must stem from other degradation processes (Fig. 4d). For example, 1,2-DCA most likely formed from 1,1,2-TCA via hydrogenolysis (Tobiszewski and Namieśnik, 2012; Vogel et al., 1987), catalyzed by Fe^0/FeOx sites (Suslick et al., 1991; Song and Carraway, 2008) that became exposed at FeS_m defect sites upon aging of the S-nZVI in the groundwater (Mangayayam et al., 2019a). This interpretation is supported by the observation that 1,2-DCA only formed after an incubation period of 100 h and to a greater extent in experiments with S-nZVI$_{0.25\ h}$, whose thinner, less crystalline FeS_m shell is more prone to aging (Fig. 4d). The formation of 1,1-DCE, on the other hand, indicated dehydrochlorination of 1,1,2-TCA (Tobiszewski and Namieśnik 2012; Song and Carraway 2008). Such a process would also explain why the 1,1-DCE concentration in the CHCs groundwater increased after ~300 h (Fig. 2d), concomitant with the decrease in 1,1,2 TCA. Note that after 150 h of monitoring, the 1,1-DCE concentration decreased again (Fig. 4d), similar to trends in the mixed CHC groundwater (Fig. 4d), indicating that it can be degraded by S-nZVI materials.

In a recent study, where S-nZVI was reacted with 1,1-DCA, 1,2-DCA and 1,1,2-TCA in single CHC reactions (no CHC competition) (Zhang et al., 2021), k_{obs} of 1,1,2-TCA was also shown to be highest amongst these chlorinated ethanes, while no reaction was observed for 1,2-DCA. Conversely to this study, they observed some 1,1-DCA degradation, as detected by the evolution of fully dechlorinated hydrocarbons and substantial amounts of vinyl chloride (VC) (Zhang et al., 2021). Here, detection of fully dechlorinated hydrocarbons and VC was not possible (due to instrument limitations). However, even if possible, it would have been difficult to identify a small extent of 1,1-DCA degradation, given some VC was already present in the CHC contaminated groundwater tested here. Overall, given the minimal reaction between S-nZVI materials and 1,1-DCA and 1,1-DCA, soil pollution containing these CHCs should probably be treated with additional methods.

3.3.3. Chlorinated methane

TCM reduction trends (Fig. 2i) were similar to observations made for cis-DCE and 1,1,2-TCA, where reduction rates inversely correlated with S-nZVI sulfidation time (i.e., k_{obs}S-nZVI$_{0.25\ h}$ > k_{obs}S-nZVI$_{2.5\ h}$ > k_{obs}S-nZVI$_{25\ h}$, Table S3). This is particularly visible at reaction times > 200 h (dashed arrow in Fig. 2i), where TCM reduction by S-nZVI$_{0.25\ h}$ (i.e., short sulfidation time) suddenly increased, while for S-nZVI$_{25\ h}$ and S-nZVI$_{2.5\ h}$ TCM reduction trends were fairly linear (Fig. S6). Previous studies have argued that TCM reduction by S-nZVI proceeds via hydrogenolysis and direct electron transfer Ghahghaei Nezamabadi (2015). As such, the sudden increase in TCM reduction by S-nZVI$_{0.25\ h}$ after 200 h may be due to the onset of hydrogenolysis enabled by the exposure of Fe^0/FeOx sites at FeS_m shell defects after some aging in the groundwater (Mangayayam et al., 2019a) as argued earlier.

3.4. Differences in S-nZVI and nZVI reactivity

S-nZVI reduction rates, k_{obs}, for all measured CHCs were higher than nZVI k_{obs}. Moreover, the sequence by which CHCs were reduced by S-nZVI (i.e., TCE > trans-DCE > 1,1-DCE > TCM > PCE > cis-DCE > 1,1,2-TCA) was distinct from the sequence observed for nZVI, where TCM was reduced the fastest. It also differs considerable from the sequence observed in single CHC reactions with S-nZVI (i.e., TCM > trans-DCE > TCE > 1,1,2-TCA > cis-DCE > PCE) in a recent study (Zhang et al., 2021), where S-nZVI was also produced by two-step synthesis with Na_2S, but then only reacted with one CHC at a time (i.e., no competition effects). Thus, in parts the difference in CHC reduction sequence between studies may be explained by CHC competition effects acting in our experiments. However, given that the nZVI material in that particular study showed no reactivity with chlorinated ethenes (i.e., TCE, PCE, cis-DCE and trans-DCE), while our nZVI material reacted with chlorinated ethenes in the groundwaters, it is also apparent that differences in CHC reduction sequence between studies is likely also due to differing S-nZVI and nZVI materials. Important to note that the reduction rates determined here may not be fully accurate because partially dechlorinated products are not accounted for, such as the possible formation of TCE from PCE or the earlier discussed formation of 1,2-DCA and 1,1-DCE from 1,1,2-TCA. However, this and recent studies show that the amount of partially dechlorinated products is actually very low or not even detected in reactions with S-nZVI (Zhang et al., 2021; Islam et al., 2020), thus it would likely not have significantly affected the S-nZVI rates presented here. For nZVI, the formation of partially dechlorinated products could have affected the rates based on previous research (Velimirovic et al., 2013; Islam et al., 2020), but given they were much lower compared to the rates determined for S-nZVI, the general trends discussed here are still valid.

In an attempt to compare CHC degradation mechanisms between nZVI and S-nZVI systems, we plotted k_{obs} values versus published values of CHCs lowest unoccupied molecular orbital (E_{LUMO}) (Fig. 5) (Scherer et al., 1998). E_{LUMO} values represent the potential of a compound to accept electrons based on its molecular configuration; thus, potential differences in these correlations could hint towards differences in electron transfer mechanisms during CHC degradation. For nZVI, an adequate linear relationship is observed between these two variables (R^2 = 0.94), which matches previous observations (Scherer et al., 1998). Assuming that mass transport does not affect reaction rates, meaning that contact between CHCs and nZVI surface sites is not limiting the reaction (Song and Carraway, 2008), the parameter that seems to predominantly affect the rate of CHC reduction by nZVI is the rate of electron transfer from nZVI to the CHC molecule governed by nZVI reduction potential. Note however, that the strong linear correlation between CHC reduction potential (i.e., E_{LUMO} values) and the pseudo-first order rate constants obtained for nZVI in this study is likely specific to the nZVI material tested here. CHC degradation trends with nZVI can vary greatly as a result of synthesis procedure (Velimirovic et al., 2013; Islam et al., 2020) and we refer the readers to earlier studies that extensively studied nZVI QSAR with CHC (Song and Carraway 2008; Scherer et al., 1998; Arnold and Roberts 1998; Chaplin et al., 2012; Miehr et al., 2004).

For S-nZVI, such a correlation between k_{obs} and E_{LUMO} is not obvious (Fig. 5). Linear correlations are also absent when the analysis is performed using other published descriptors of reduction potential such as one-electron or two-electron reduction potential (Fig. S7) (Tobiszewski and Namieśnik 2012). Parameters such as partitioning coefficients (i.e., gas-liquid, octanol-water) and CHCs concentrations were also tested but a correlation with any of these parameters was also lacking (Fig. S8) (Stroo and Ward 2010).

The lack of any trends between k_{obs} values and CHC properties in S-nZVI reactions could indicate that S-nZVI reactivity towards the different CHCs is to a significant extent controlled by the heterogeneity of S-nZVI surface sites (i.e., FeS_m and Fe^0/FeOx). For example, k_{obs} for 1,1-DCE and trans-DCE were highest for S-nZVI with a thick and crystalline FeS_m shell, while cis-DCE could not be reduced at FeS_m surface sites. These observations suggest that FeS_m surface sites may have specific binding affinities for specific CHC molecular geometries, considering that these compounds have different stereochemistry but comparable reduction potentials (Table S4). Additionally, we showed that TCE was reduced the fastest by S-nZVI (e.g., TCE k_{obs} up to 3-fold higher than trans-DCE k_{obs}) and not affected by the presence of site competitive CHCs (e.g., 1,1,2-TCA), suggesting that TCE reduction is highly favoured at FeS_m surface sites. Further complexity is added by the fact that S-nZVI materials eventually also expose some Fe^0/FeOx surface sites, once S-nZVI have been aged in water (Mangayayam et al., 2019a).

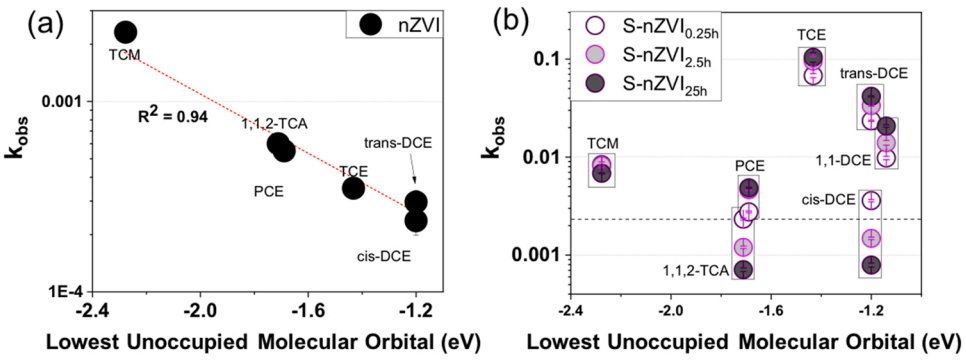

Fig. 5. Trends between CHC reduction rate constants, k_{obs}, and CHC E_{LUMO} (values obtained from Scherer et al., (1998) for reactions with a) nZVI and b) S-nZVI materials sulfidated for different time lengths (y-axis in log scale). In (a) the dashed line shows the linear fit (R^2 = 0.94) between k_{obs} and E_{LUMO}. In (b) the dashed line shows the highest k_{obs} value measured in nZVI reactions (i.e., TCM k_{obs}) and the boxes delineate the range of k_{obs} for each CHC compound as a function S-nZVI sulfidation time. Error bars represent standard error of the linear regression fitting to obtain k_{obs}.

This behavior was distinctly observed for S-nZVI$_{0.25\,h}$ that has a thinner and less crystalline FeS_m shells, which arguably leads to exposure of more Fe^0/FeOx sites compared to the more sulfidated S-nZVI, S-nZVI$_{25\,h}$. For instance, we showed relatively faster reduction of 1,1,2-TCA, TCM and cis-DCE with S-nZVI$_{0.25\,h}$ compared to S-nZVI$_{25\,h}$, which happened after a certain incubation time, i.e., once Fe^0/FeOx sites became exposed. The gradual exposure of Fe^0/FeOx sites with aging seems particularly important to enable cis-DCE reduction, which does not readily occur at FeS_m sites, as shown here and previously (Mangayayam et al., 2019b; Jeong et al., 2011; Hyun and Hayes 2015). Noteworthy, that for some S-nZVI materials, cis-DCE reduction was shown to be higher than for nZVI (Zhang et al., 2021; Islam et al., 2020). This may be explained by those studies using a lower S/Fe_{dosed} ratio (0.05 vs. 0.23 used here) and a different nZVI precursor and sulfidation treatment compared to this study.

Overall, while sulfidation seems to bring a number of improved surface properties for CHC degradation (i.e., reduced anaerobic oxidation and corrosion, higher electron conductivity and hydrophobicity, lower wettability, etc.), that enhance degradation rates of individual CHC compounds compared to non-sulfidated nZVI (Fan et al., 2016; Nunez Garcia et al., 2021), none of these parameters alone can explain the varied extent of rate enhancement observed among different CHCs in these complex groundwaters. Such a conclusion was also presented by Zhang et al. (2021) when explaining the varied reduction trends observed for chlorinated ethenes by S-nZVI when compared to chlorinated ethanes and methanes.

On a last note given that cis-DCE has been shown to be quickly reduced at Fe^0/FeOx sites (Burke and Madix, 1990; Arnold and Roberts, 1998; Lampron, 2001), it may be surprising that cis-DCE reduction by nZVI was relatively slow in nZVI reactions here. We explain this by nZVI favouring the reduction of TCM and 1,1,2-TCA over cis-DCE, consistent with their respective E_{LUMO} values (Fig. 5a). Also, TCM and 1,1,2-TCA degradation were still ongoing at the end of nZVI reactions (Fig. 2h, i), thus no significant cis-DCE could take place.

4. Conclusions

We have demonstrated that an increase in sulfidation time increases the thickness and crystallinity of the mackinawite-like (FeS_m) shell for two-step synthesised S-nZVI with Na_2S, which in turn increases the stability and abundance of FeS_m surface sites, and thereby significantly alters reactivity of S-nZVI with CHCs. Specifically, reduction rates of PCE, TCE, trans-DCE, and 1,1-DCE were highest for the S-nZVI material with the most crystalline and thickest FeS_m shell, while rates for cis-DCE, 1,1,2-TCA, and TCM were highest for the S-nZVI material with the least crystalline and thinnest FeS_m shell. These trends suggest that PCE, TCE, trans-DCE, and 1,1-DCE have a relatively high affinity for FeS_m sites, and can be reduced at this sites. This affinity towards FeS_m sites seems however, lower for cis-DCE, 1,1,2-TCA, and TCM, but our data suggest they can still be degraded at these sites, particularly 1,1,2-TCA and TCM. However, because these CHCs are also effectively reduced at Fe^0/FeO_x sites, we generally observed an increase in their degradation after some incubation time, i.e., aging, that allowed for Fe^0/FeO_x sites to become accessible at defects sites in the FeS_m shell. Also, a thinner, less crystalline FeS_m surface as in S-nZVI$_{0.25\,h}$ seems to expose more Fe^0/FeO_x sites with aging due to the relatively lower structural integrity of the FeS shell surrounding Fe^0 core.

In comparison to nZVI, dechlorination rates by S-nZVI materials were up to two magnitudes higher but unlike nZVI, S-nZVI materials did not reduce the CHCs according to their reduction potential. Instead, the presence and heterogeneity of surface FeS_m and Fe^0/FeOx sites seem to control how fast or slow CHCs are degraded. It is noted that when nZVI is added to the contaminated groundwater, FeOx sites quickly form on the nZVI surface. However, this process seems to passivate rather than promote electron transfer leading to lower reactivity.

Overall, these results could help towards strategic design of S-nZVI materials to fit specific CHC treatment scenarios. As an example, S-nZVI with a thick, crystalline FeS_m shell seems most suitable for treatment of source zones, which typically consist of fully chlorinated or unsaturated CHCs (i.e., PCE, TCE). On the other hand, S-nZVI with a thin, less crystalline FeS_m shell would be more suitable for treatment of CHC groundwater plumes, which generally exhibit a more complex mixture of compounds (cis-DCE, DCA), due to partial natural attenuation.

Novelty statement

This is the first study to analyse the reactivity and selectivity of different S-nZVI materials and nZVI towards chlorinated hydrocarbons (CHC) in a real CHC contaminated groundwater with more than 9 co-existing CHC compounds. Comparison of S-nZVI and nZVI reactivity trends with CHC reduction potential shows a linear correlation for nZVI but not for S-nZVI. We also show that the FeS shell of S-nZVI induces selectivity towards CHC compounds, explained by the heterogeneity of its surface sites (i.e., FeS and Fe^0/FeOx). Overall, these results provide key new information to help guide S-nZVI synthesis for remediation of specific CHC contaminantion scenarios.

CRediT authorship contribution statement

Marco C. Mangayayam: Conceptualization, Methodology, Investigation, Writing – original draft. **Jeffrey Paulo H. Perez:** Investigation, Writing – review & editing. **Virginia Alonso-de-Linaje:** Resources, Writing – review & editing. **Knud Dideriksen:** Supervision, Funding acquisition, Writing – review & editing. **Liane G. Benning:** Supervision, Funding acquisition, Writing – review & editing. **Dominique J. Tobler:** Supervision, Funding acquisition, Project administration, Writing – review & editing.

Declaration of Competing Interest

The authors declare that they have no known competing financial interests or personal relationships that could have appeared to influence

the work reported in this paper.

Acknowledgements

This research was funded by Metal-Aid Innovative Training Network (ITN), supported by a grant from the European Commission's Marie Skłowdowska Curie Actions Program under project number 675219. The authors thank Theis Brock-Nannestad for support with GC-MS measurements. LGB and JPHP acknowledge the financial support of the Helmholtz Recruiting Initiative grant No. I-044-16-01. Part of the data was acquired at Advanced Photon Source, a U.S. Department of Energy (DOE) Office of Science User Facility operated for the DOE Office of Science by Argonne National Laboratory under contract no. DE-AC02-06CH11357. Support for travel to the synchrotron facility came from the Danish Council for Independent Research (via DANSCATT).

Appendix A. Supporting information

Supplementary data associated with this article can be found in the online version at doi:10.1016/j.jhazmat.2022.128534.

References

Alonso-de-Linaje, V., Mangayayam, M.C., Tobler, D.J., Dietmann, K.M., Espinosa, R., Rives, V., Dalby, K.N., 2019. Sorption of chlorinated hydrocarbons from synthetic and natural groundwater by organo-hydrotalcites: towards their applications as remediation nanoparticles. Chemosphere 236 (124369).

Arnold, W.A., Roberts, Lynn, 1998. A pathways of chlorinated ethylene and chlorinated acetylene reaction with Zn(O). Environ. Sci. Technol. 32 (19), 3017–3025.

Bae, S., Collins, R.N., Waite, T.D., Hanna, K., 2018. Advances in surface passivation of nanoscale zerovalent iron: a critical review. Environ. Sci. Technol. 52 (21), 12010–12025.

Barrio-Lage, G., Parsons, F.Z., Nassar, R.S., Lorenzo, P.A., 1986. Sequential dehalogenation of chlorinated ethenes. Environ. Sci. Technol. 20 (1), 96–99.

Bartholomew, C.H., Agrawal, P.K., Katzer, J.R., 1982. Sulfur Poisoning of Metals. In: Eley, D.D., Pines, H., Weisz, P.B. (Eds.), Advances in Catalysis, 31. Academic Press, pp. 135–242.

Brumovský, M., Filip, J., Malina, O., Oborná, J., Sracek, O., Reichenauer, T.G., Andrýsková, P., Zbořil, R., 2020. Core–shell Fe/FeS nanoparticles with controlled shell thickness for enhanced trichloroethylene removal. ACS Appl. Mater. Interfaces 12 (31), 35424–35434.

Burke, M.L., Madix, R.J., 1990. Hydrogen on Pd(100)-S: The Effect of Sulfur on Precursor Mediated Adsorption and Desorption. Surf. Sci. 237, 1–19.

Cao, Z., Li, H., Zhang, S., Hu, Y., Xu, J., Xu, X., 2021. Properties and reactivity of sulfidized nanoscale zero-valent iron prepared with different borohydride amounts. Environ. Sci. Nano 8 (9), 2607–2617.

Chaplin, B.P., Reinhard, M., Schneider, W.F., Schüth, C., Shapley, J.R., Strathmann, T.J., Werth, C.J., 2012. Critical review of Pd-based catalytic treatment of priority contaminants in water. Environ. Sci. Technol. 46 (7), 3655–3670.

Fan, D., O'Brien Johnson, G., Tratnyek, P.G., Johnson, R.L., 2016. Sulfidation of nano zerovalent Iron (NZVI) for improved selectivity during in-situ chemical reduction (ISCR). Environ. Sci. Technol. 50 (17), 9558–9565.

Ghahghaei Nezamabadi, S., 2015. Accelerated Degradation of Chlorinated Solvents by Nanoscale Zero-Valent Iron Coated with Iron Monosulfide and Stabilized with Carboxymethyl Cellulose. Wright University.

Gu, Y., Wang, B., He, F., Bradley, M.J., Tratnyek, P.G., 2017. Mechanochemically sulfidated microscale zero valent iron: pathways, kinetics, mechanism, and efficiency of trichloroethylene dechlorination. Environ. Sci. Technol. 51 (21), 12653–12662.

He, F., Li, Z., Shi, S., Xu, W., Sheng, H., Gu, Y., Jiang, Y., Xi, B., 2018. Dechlorination of excess trichloroethene by bimetallic and sulfidated nanoscale zero-valent iron. Environ. Sci. Technol. 52 (15), 8627–8637.

Hyun, S.P., Hayes, K.F., 2015. Abiotic reductive dechlorination of Cis-DCE by ferrous monosulfide mackinawite. Environ. Sci. Pollut. Res. 22 (21), 16463–16474.

Islam, S., Han, Y., Yan, W., 2020. Reactions of chlorinated ethenes with surface-sulfidated iron materials: reactivity enhancement and inhibition effects. Environ. Sci. Process Impacts 22 (3), 759–770.

Jeong, H.Y., Anantharaman, K., Han, Y.S., Hayes, K.F., 2011. Abiotic reductive dechlorination of Cis -dichloroethylene by Fe species formed during iron- or sulfate-reduction. Environ. Sci. Technol. 45 (12), 5186–5194.

Kim, E.J., Kim, J.H., Azad, A.M., Chang, Y.S., 2011. Facile synthesis and characterization of Fe/FeS nanoparticles for environmental applications. ACS Appl. Mater. Interfaces 3 (5), 1457–1462.

Lampron, K., 2001. Reductive dehalogenation of chlorinated ethenes with elemental iron: the role of microorganisms. Water Res. 35 (13), 3077.

Lawrence, S.J. 2006. Description, Properties, and Degradation of Selected Volatile Organic Compounds Detected in Ground Water — A Review of Selected Literature; Atlanta, Georgia, U. S. Geological Survey, Open-File Report 2006-1338, 62p.

Mangayayam, M.C., Dideriksen, K., Ceccato, M., Tobler, D.J., 2019b. The structure of sulfidated zero-valent iron by one-pot synthesis: impact on contaminant selectivity and long-term performance. Environ. Sci. Technol. 53 (8), 4389–4396.

Mangayayam, M.C., Perez, J.P.H., Dideriksen, K., Freeman, H.M., Bovet, N., Benning, L. G., Tobler, D.J., 2019a. Structural transformation of sulfidated zerovalent iron and its impact on long-term reactivity. Environ. Sci. Nano 6 (11), 3422–3430.

Middeldorp, P.J.M., Luijten, M.L.G.C., Pas, B.A., van de, Eekert, M.H.A., van, Kengen, S. W.M., Schraa, G., Stams, A.J.M., 1999. Anaerobic microbial reductive dehalogenation of chlorinated ethenes. Bioremed. J. 3 (3), 151–169.

Miehr, R., Tratnyek, P.G., Bandstra, J.Z., Scherer, M.M., Alowitz, M.J., Bylaska, E.J., 2004. Diversity of contaminant reduction reactions by zerovalent iron: role of the reductate. Environ. Sci. Technol. 38 (1), 139–147.

Moran, M.J., Zogorski, J.S., Squillace, P.J., 2007. Chlorinated solvents in groundwater of the United States. Environ. Sci. Technol. 41 (1), 74–81.

Mueller, N.C., Braun, J., Bruns, J., Černík, M., Rissing, P., Rickerby, D., Nowack, B., 2012. Application of nanoscale zero valent iron (NZVI) for groundwater remediation in Europe. Environ. Sci. Pollut. Res. 19 (2), 550–558.

Nunez Garcia, A., Boparai, H.K., Ocarroll, D.M., 2016. Enhanced dechlorination of 1,2-dichloroethane by coupled nano iron-dithionite treatment. Environ. Sci. Technol. 50 (10), 5243–5251.

Nunez Garcia, A., Boparai, H.K., Chowdhury, A.I.A., de Boer, C.V., Kocur, C., Passeport, E., Lollar, B.S., Austrins, L.M., Herrera, J., O'Carroll, D.M., 2020. Sulfidated nano zerovalent iron (S-nZVI) for in situ treatment of chlorinated solvents: a field study. Water Res. 174, 115594.

Nunez Garcia, A.N., Zhang, Y., Ghoshal, S., He, F., O'Carroll, D.M., 2021. Recent advances in sulfidated zerovalent iron for contaminant transformation. Environ. Sci. Technol. 55 (13), 8464–8483.

Phenrat, T., Lowry, G.V., Babakhani, P., 2019. Nanoscale zerovalent Iron (NZVI) for environmental decontamination: a brief history of 20 years of research and field-scale application. In: Phenrat, T., Lowry, G.V. (Eds.), Nanoscale Zerovalent Iron Particles for Environmental Restoration: From Fundamental Science to Field Scale Engineering Applications. Springer International Publishing, Cham, pp. 1–43.

Rajajayavel, S.R.C., Ghoshal, S., 2015. Enhanced reductive dechlorination of trichloroethylene by sulfidated nanoscale zerovalent iron. Water Res. 78, 144–153.

Reardon, E.J., 2005. Zerovalent irons: styles of corrosion and inorganic control on hydrogen pressure buildup. Environ. Sci. Technol. 39 (18), 7311–7317.

Scherer, M.M., Balko, B.A., Gallagher, D.A., Tratnyek, P.G., 1998. Correlation analysis of rate constants for dechlorination by zero-valent iron. Environ. Sci. Technol. 32 (19), 3026–3033.

Song, H., Carraway, E.R., 2005. Reduction of chlorinated ethanes by nanosized zero-valent iron: kinetics, pathways, and effects of reaction conditions. Environ. Sci. Technol. 39 (16), 6237–6245.

Song, H., Carraway, E.R., 2008. Catalytic hydrodechlorination of chlorinated ethenes by nanoscale zero-valent iron. Appl. Catal. B Environ. 78 (1–2), 53–60.

Stefaniuk, M., Oleszczuk, P., Ok, Y.S., 2016. Review on nano zerovalent iron (NZVI): from synthesis to environmental applications. Chem. Eng. J. 287, 618–632.

Stroo, H.F., Ward, C.H., 2010. In situ remediation of chlorinated solvent plumes. In: Stroo, H.F., Ward, C.H. (Eds.), SERDP/ESTCP Environmental Remediation Technology. Springer New York, New York, NY.

Suslick, K.S., Choe, S.B., Cichowlas, A.A., Grinstaff, M.W., 1991. Sonochemical synthesis of amorphous iron. Nature 353 (6343), 414–416.

Tobiszewski, M., Namieśnik, J., 2012. Abiotic degradation of chlorinated ethanes and ethenes in water. Environ. Sci. Pollut. Res. 19 (6), 1994–2006.

Velimirovic, M., Larsson, P.O., Simons, Q., Bastiaens, L., 2013. Reactivity screening of microscale zerovalent irons and iron sulfides towards different CAHs under standardized experimental conditions. J. Hazard Mater. 252–253, 204–212. May 15.

Vogan, J.L., Focht, R.M., Clark, D.K., Graham, S.L., 1999. Performance evaluation of a permeable reactive barrier for remediation of dissolved chlorinated solvents in groundwater. J. Hazard. Mater. 68 (1–2), 97–108.

Vogel, T.M., Criddle, C.S., McCarty, P.L., Arcos, J.C., 1987. Transformations of halogenated aliphatic compounds: oxidation, reduction, substitution, and dehydrohalogenation reactions occur abiotically or in microbial and mammalian systems. Environ. Sci. Technol. 21 (8), 722–736.

Xu, J., Cao, Z., Zhou, H., Lou, Z., Wang, Y., Xu, X., Lowry, G.V., 2019. Sulfur dose and sulfidation time affect reactivity and selectivity of post-sulfidated nanoscale zerovalent iron. Environ. Sci. Technol. 53 (22), 13344–13352.

Xu, J., Avellan, A., Li, H., Liu, X., Noël, V., Lou, Z., Wang, Y., Kaegi, R., Henkelman, G., Lowry, G.V., 2020. Sulfur loading and speciation control the hydrophobicity, electron transfer, reactivity, and selectivity of sulfidized nanoscale zerovalent iron. Adv. Mater. 32 (17), 1906910.

Zhang, Y., Ozcer, P., Ghoshal, S., 2021. A comprehensive assessment of the degradation of C1 and C2 chlorinated hydrocarbons by sulfidated nanoscale zerovalent iron. Water Res. 201, 117328.